



## Article

# Epithelial Sodium Channel Alpha Subunit ( $\alpha$ ENaC) Is Associated with Inverse Salt Sensitivity of Blood Pressure

Peng Xu <sup>1</sup>, Anastasia V. Sudarikova <sup>2,3</sup> , Daria V. Ilatovskaya <sup>2,4</sup>, John J. Gildea <sup>1</sup>, Mahabuba Akhter <sup>5</sup>, Robert M. Carey <sup>5</sup> , Wei Yue <sup>1</sup> , Pedro A. Jose <sup>6</sup> and Robin A. Felder <sup>1,\*</sup>

- <sup>1</sup> Department of Pathology, University of Virginia Health System, Charlottesville, VA 22903, USA; px3x@virginia.edu (P.X.); jjg5b@virginia.edu (J.J.G.); wy9c@hscmail.mcc.virginia.edu (W.Y.)
- <sup>2</sup> Division of Nephrology, Department of Medicine, Medical University of South Carolina, Charleston, SC 29425, USA; anastasia.sударикова@gmail.com (A.V.S.); dilatovskaya@augusta.edu (D.V.I.)
- <sup>3</sup> Institute of Cytology, Russian Academy of Sciences, 194064 St. Petersburg, Russia
- <sup>4</sup> Department of Physiology, Medical College of Georgia, Augusta University, Augusta, GA 30912, USA
- <sup>5</sup> Division of Endocrinology and Metabolism, Department of Medicine, University of Virginia Health System, Charlottesville, VA 22903, USA; ma5u@hscmail.mcc.virginia.edu (M.A.); rmc4c@hscmail.mcc.virginia.edu (R.M.C.)
- <sup>6</sup> School of Medicine and Health Sciences, The George Washington University, Washington, DC 20052, USA; pjose@mfa.gwu.edu
- \* Correspondence: robin@virginia.edu; Tel.: +1-434-924-5151



**Citation:** Xu, P.; Sudarikova, A.V.; Ilatovskaya, D.V.; Gildea, J.J.; Akhter, M.; Carey, R.M.; Yue, W.; Jose, P.A.; Felder, R.A. Epithelial Sodium Channel Alpha Subunit ( $\alpha$ ENaC) Is Associated with Inverse Salt Sensitivity of Blood Pressure. *Biomedicines* **2022**, *10*, 981. <https://doi.org/10.3390/biomedicines10050981>

Academic Editors: Sheng-Nan Wu and Jun Lu

Received: 18 February 2022

Accepted: 20 April 2022

Published: 23 April 2022

**Publisher's Note:** MDPI stays neutral with regard to jurisdictional claims in published maps and institutional affiliations.



**Copyright:** © 2022 by the authors. Licensee MDPI, Basel, Switzerland. This article is an open access article distributed under the terms and conditions of the Creative Commons Attribution (CC BY) license (<https://creativecommons.org/licenses/by/4.0/>).

**Abstract:** Salt sensitivity of blood pressure (BP) refers to an increase in BP following an increase in dietary salt, which is associated with increased incidence of cardiovascular disease and early death. However, decreased sodium intake also increases mortality and morbidity. Inverse salt sensitivity (ISS), defined as a paradoxical increase in BP on a low-salt diet, about 11% of the population, may be the cause of this phenomenon. The epithelial sodium channel (ENaC) is a major regulator of sodium reabsorption in the kidney. In this study, human renal tubular epithelial cells (hRTC) were cultured from the urine of phenotyped salt study participants.  $\alpha$ ENaC expression was significantly lower in ISS than salt resistant (SR) hRTC, while ENaC-like channel activity was dramatically increased by trypsin treatment in ISS cells analyzed by patch clamp.  $\alpha$ ENaC expression was also decreased under high-salt treatment and increased by aldosterone treatment in ISS cells. Moreover, the  $\alpha$ ENaC variant, rs4764586, was more prevalent in ISS. In summary,  $\alpha$ ENaC may be associated with ISS hypertension on low salt. These findings may contribute to understanding the mechanisms of ISS and low salt effect on morbidity and mortality.

**Keywords:** aldosterone; ENaC; inverse salt sensitivity; patch clamp; salt resistance; salt sensitivity

## 1. Introduction

The amiloride-sensitive epithelial sodium channel (ENaC) is located mostly in the apical membrane of epithelial cells of the lung, distal nephron, distal colon, and ducts of exocrine glands [1]. As a non-voltage gated ion channel, ENaC constitutively allows the flow of luminal  $\text{Na}^+$  ions across the apical cell membrane into epithelia cells [2–4]. ENaC is a heterotrimeric complex comprised of three homologous subunits,  $\alpha$ ,  $\beta$ , and  $\gamma$  [1,5]. Each subunit contains two transmembrane domains, an extracellular loop, and an intracellular N- and C-termini [5–7]. Renal ENaC plays an important role in the regulation of whole-body  $\text{Na}^+$  hemostasis and the control of blood pressure (BP). It acts as a key regulator of sodium reabsorption in distal convoluted tubule (DCT), connecting tubule (CNT), and principal collecting duct (CD) [8,9]. In the kidney, the expression and activity of ENaC in the distal nephron is under the control of aldosterone and antidiuretic hormone, which are essential regulators of BP [10,11].

Abnormalities in ENaC expression or function are associated with human pathology. Genetic deletion or loss-of-function mutations in any ENaC subunit cause pseudohypoaldosteronism type 1 (PHA-1) which is characterized by  $\text{Na}^+$  wasting [12–15]. Global inactivation of  $\alpha$ ,  $\beta$ , or  $\gamma$ ENaC causes death after birth [16–18]. CD-specific  $\alpha$ ENaC KO mice are able to maintain sodium and potassium balance when subjected to low  $\text{Na}^+$  or high  $\text{K}^+$  feeding [19]. However, when  $\alpha$ ENaC is knocked out in both the CD and CNT, mice develop mild hyponatremia and hyperkalemia when fed a standard diet as well as a significant reduction of body weight during  $\text{Na}^+$  restriction [20]. The GenSalt study reported that one rare variant of  $\alpha$ ENaC, rs4764586, was associated with an increased likelihood of salt sensitivity of BP [21]. Salt sensitivity is a quantitative trait, defined as an increase of BP in response to an increase in  $\text{Na}^+$  load [22–25], but not necessarily to hypertensive levels. By contrast, we found inverse salt sensitive (ISS) individuals show increased BP under low salt intake and require high salt intake in order to maintain a normal BP [24,26]. As ENaC plays an important role in regulating  $\text{Na}^+$  balance, we hypothesized that ENaC may differentially regulate  $\text{Na}^+$  transport in salt resistant (SR) and ISS individuals. In order to test this hypothesis, we measured the presence of ENaC in CD13-positive renal cells collected from the urine of our dietary salt study participants who were ultimately phenotyped for their BP response to randomized transitions between week-long high (300 mEq) and low (10 mEq)  $\text{Na}^+$  diets [24]. Patch clamp electrophysiology was used to measure single-channel ENaC-like activity in cells from SR and ISS individuals. The role of aldosterone in regulating  $\alpha$ ENaC was also examined.

## 2. Materials and Methods

### 2.1. Cohort Stratification

Specimens were collected from volunteer participants enrolled in an Institutional Review Board-approved dietary salt study [24]. The participants ( $n = 280$ ) were grouped into three classes, depending on the BPs obtained after 14 days of diets prepared by a dietician in the University of Virginia Medical Center containing 10 mEq  $\text{Na}^+$  (as NaCl) and 300 mEq  $\text{Na}^+$  (Supplemental Table S1). The BP measurement was described in a previous paper [24]. Briefly, the BP was measured every 15 min, 3 times at the right arm in the sitting position during each visit. There were 7 visits in total during the 2-week diet phase. The BPs on the 4th and 7th visits, at the end of the low- or high-salt diet, were used to calculate mean arterial pressure (MAP). The change in delta ( $\Delta$ ) MAP was defined as the MAP on the last day of the high  $\text{Na}^+$  diet minus the MAP on the last day of the low  $\text{Na}^+$  diet. The subjects were classified into SR (64% of participants) if they had an increase in MAP of  $<7$  mmHg on 300 mEq  $\text{Na}^+$  intake and a decrease in MAP of  $<7$  mmHg on 10 mEq  $\text{Na}^+$  intake [24]; SS (23% of participants) had an increase in MAP  $\geq 7$  mmHg on 300 mEq  $\text{Na}^+$  intake and a decrease in MAP  $\geq 7$  mmHg on 10 mEq  $\text{Na}^+$  intake [24]; and ISS (13% of participants) had a decrease in MAP  $\geq 7$  mmHg on 300 mEq  $\text{Na}^+$  intake and an increase in MAP  $\geq 7$  mmHg on a 10 mEq  $\text{Na}^+$  intake [24,26].

### 2.2. Cells from Human Urine

Human renal tubule cells (hRTCs) were collected from urine freshly voided by participants on regular diet in our clinical study as described in our previous study [27]. The cells were then briefly rinsed once by PBS++ (D8662, Sigma-Aldrich, St. Louis, MO, USA) and centrifuged at  $1000 \times g$  for 3 min. Finally, the cells were plated in a 6-well plate and cultured in renal epithelial cell growth basal medium (REBM, cc-3190, Lonza, Walkersville, MD, USA) at  $37^\circ\text{C}$  in 5%  $\text{CO}_2$ –95% air atmosphere [27,28]. In about 2 weeks, cell colonies were visible. The cells were immortalized by human telomerase reverse transcriptase (tert) [27]. We have previously shown that renal cells voided in the urine demonstrate a natriuretic phenotype that matches their kidney's ability to appropriately eliminate sodium, and the cells continue to express their phenotype up to 10 years after being phenotyped [29].

### 2.3. AutoMACS Selection and Flow Cytometry

Cells were grown in 15-cm dishes to 85% confluence ( $\sim 10^7$ ) and then trypsinized, filtered using a 30- $\mu\text{m}$  filter, and centrifuged at  $1000\times g$  for 3 min. The pelleted cells were rinsed with cold MACS buffer (Miltenyi Biotec, Boston, MA, USA), and re-centrifuged at  $1000\times g$  for 3 min. The supernatant was discarded, 100  $\mu\text{L}$  of MACS Buffer (130-091-221, Miltenyi Biotec) was added, and the suspension was transferred to a 1.5-mL tube with 5  $\mu\text{L}$  of CD13-PE (347837, BD Biosciences, San Jose, CA, USA). After mixing, the cells, protected from light, were incubated at 4  $^{\circ}\text{C}$  for 20 min, and then 1 mL of MACS Buffer was added, mixed well, and centrifuged at  $1000\times g$  for 3 min. The pelleted cells were then resuspended in 100  $\mu\text{L}$  MACS Buffer mixed with 10  $\mu\text{L}$  anti-PE magnetic beads (Miltenyi Biotec) for 20 min at 4  $^{\circ}\text{C}$ . The cells were rinsed, collected and finally resuspended in 500  $\mu\text{L}$  MACS Buffer and transferred to a 5 mL tube that was kept on ice and protected from light. The cells were purified to near homogeneity using an AutoMACS (Miltenyi Biotec) for selection, using a single column. Positive and negative fractions were measured by flow cytometry (BD Accuri C6, BD Biosciences, San Jose, CA, USA).

### 2.4. Immunofluorescence Staining

The hRTCs were plated in collagen-coated 96-well glass-bottom plates. After the cells grew to 80–90% confluence, they were fixed with 4% paraformaldehyde in PBS with or without 0.2% Triton for 5 min and stained as previously described [27]. The primary antibodies in Odyssey blocking buffer were tested: L1-CAM (ab24345, 1:500, Abcam, Cambridge, MA, USA); phycoerythrin (PE)-conjugated CD13 (1:50); rabbit anti- $\alpha\text{ENAC}$  (SPC-403, 1:200, StressMarq, Victoria, BC, Canada); rabbit anti- $\beta\text{ENaC}$  (SPC-404, 1:200, StressMarq Biosciences); rabbit anti- $\gamma\text{ENaC}$  (SPC-405, 1:200, StressMarq); and mouse anti-mineralocorticoid R (MR, MAB4369-SP, 1:200, R&D, Minneapolis, MN, USA). The appropriate secondary antibodies were used: Alexa Fluor 488 (1:500, Thermo Fisher Scientific, Waltham, MA, USA) and Alexa Fluor 647 (1:500, Thermo Fisher). Hoechst 33,342 (735969, 1:2000, Thermo Fisher) was used to stain the nuclei.

Human kidney cortical tissue was processed and immunofluorescence stained following the previously published procedure [27]. Anti-rabbit  $\alpha\text{ENAC}$  (SPC-403, 1:200, StressMarq; ASC-030, 1:200, Alomone Labs, Jerusalem, Israel), anti-rabbit  $\beta\text{ENaC}$  (SPC-404, 1:200, StressMarq; ab28668, 1:200, Abcam), anti-rabbit  $\gamma\text{ENaC}$  (SPC-405, 1:200 StressMarq; ab3468, 1:200, Abcam), anti-mouse L1-CAM (1:500, Abcam), LTA (FL-1321, 1:500, Vector Laboratories, Burlingame, CA, USA), secondary antibodies (anti-rabbit Alexa Fluor 488 and anti-mouse Alexa Fluor 647, 1:500, Thermo Fisher) were used.

### 2.5. Confocal Microscopy

Confocal microscopy was performed using an IX81 spinning disk confocal with both mercury and xenon light sources and Semrock hard-coated filters in a Sedat configuration (Olympus, Tokyo, Japan). Images were acquired using a 20 $\times$  and a 60 $\times$  UPlanSApo water immersion objectives for tissue section and cell imaging. The microscope was controlled by Metamorph software (BioVision Technologies, Exton, PA, USA), which can stitch single images together to obtain a view of a larger number of cells.

### 2.6. $\alpha\text{ENAC}$ siRNA Knock-Down in Cells

The hRTCs were plated in 6-well plates and grown to 50% confluent. Human  $\alpha\text{ENAC}$  siRNA (M-006504-01-0005, Dharmacon, Cambridge, UK) was mixed with Lipofectamine RNAiMAX (13778075, Thermo Fisher, Waltham, MA, USA) for 20 min at room temperature. The mixture was then added to the cells at a final siRNA concentration of 100 nM. The cells were incubated at 37  $^{\circ}\text{C}$  in a 5%  $\text{CO}_2$  incubator for 24 h. Then, the medium was changed and the cells incubated for an additional 24 h. Non-targeting siRNA (Scramble, D-001210-02-50, Dharmacon) was used as control. At the end of the additional 24 h of incubation, the cells were harvested and prepared for Western blotting.

### 2.7. Western Blot

The hRTCs (90% confluent, 6-well plate) were lysed in M-PER mammalian protein extraction buffer (78501, Thermo Fisher) and sonicated. The total protein in supernatant was measured by Bradford assay (Bio-Rad Laboratories, Hercules, CA, USA), and the proteins in the samples were separated by SDS-PAGE (4–20% gradient gel). Western blotting was performed, as previously described [27]. Rabbit anti- $\alpha$ ENaC (HPA012743, 1:500, Sigma-Aldrich; SPC-403, 1:500, StressMarq), rabbit anti- $\beta$ ENaC (ab28668, 1:500, Abcam), rabbit anti- $\gamma$ ENaC (ab3468, 1:500, Abcam), mouse anti- $\beta$ -actin (sc-517582, 1:1000, Santa Cruz, Dallas, TX, USA), and secondary antibodies (anti-rabbit IRDye 800 or anti-mouse IRDye 680, both at 1:15,000, LI-COR, Lincoln, NE, USA) were used. Fluorescence was imaged using a Bio-Rad Imager.

### 2.8. SNP Selection and Genotyping

Three  $\alpha$ ENaC SNPs, rs11614164, rs3741914, and rs4764586, which are associated with salt-sensitive BP, were chosen for genotyping [21] the human gDNA from the clinical cohort [24], using TaqMan SNP Genotyping Assay (Thermo Fisher). There were 280 samples; 37 were ISS subjects, 178 were SR subjects, and 65 were SS subjects.

### 2.9. Cell-Attached Configuration of Patch Clamp

Ion currents through single channels were recorded using cell-attached configuration of patch-clamp technique, based on Axopatch 200B amplifier, Analog-Digital Interface Digidata 1550B (Molecular Devices, CA, USA) and controlled by pClamp 10.7 software [30]. A Bessel filter (300 Hz) was used during the experiments. Patch pipettes were made from borosilicate glass BF-150-110-10 using P-97 puller (Sutter Instrument, Novato, CA, USA). The currents were recorded in a range of membrane potentials from  $-10$  to  $-60$  mV using a gap-free protocol. Extracellular pipette solution contained (mM) 140 LiCl, 5 MgCl<sub>2</sub>, 10 HEPES/Tris, pH 7.3; trypsin (5  $\mu$ g/mL) was added in order to increase ENaC activity. In one set of experiments Li<sup>+</sup> was replaced by Na<sup>+</sup> in the pipette solution. Extracellular bath solution (in the chamber) contained (mM) 150 NaCl, 5 KCl, 5 glucose, 1 CaCl<sub>2</sub>, 2 MgCl<sub>2</sub>, 10 mM HEPES, pH 7.3. To quantify the level of channel activity, we used ClampFit software processing, and the following equation was used to define Po:  $P_o = I/Ni$ , where Po—channel open probability, N—number of working channels in the patch, I—the mean current determined from the amplitude histograms, i—unitary current amplitude.

### 2.10. Aldosterone Treatment

hRTCs from SR and ISS subjects were plated in 96-well glass bottom plates, and then treated overnight with 1  $\mu$ M aldosterone at 37 °C (1  $\mu$ M aldosterone was chosen by the concentration that provided a 50% increase in total aldosterone response). The hRTCs were fixed and stained with mouse anti-mineralocorticoid receptor antibody (R&D MAB4369-SP, 1:200) and  $\alpha$ ENaC (SPC-403, 1:200, StressMarq). Montage images of each well were obtained under 20 $\times$  using a Cytation 5 image reader automatically and analyzed by Gen5 software (BioTek Instrument, Winooski, VT, USA) using MR (green) as the primary mask and  $\alpha$ ENaC (red) as the secondary mask. Cell number was counted and mean value of the fluorescence density (relative fluorescence unit RFU) was used to conduct analysis. Plasma aldosterone and plasma renin activity (PRA) were measured using clinically approved diagnostic tests available through the UVA clinical laboratory.

### 2.11. Statistical Analysis

Data were expressed as means  $\pm$  SE. Comparisons within and among groups (>2) were analyzed by repeated-measures or factorial ANOVA, respectively, followed by Tukey's (comparing every mean with every other mean), Dunnet's (comparing each mean with the other mean in that row), or Sidak's post hoc test (comparing each mean with the control mean in that column) using GraphPad Prism 7.0 software (GraphPad Software, La Jolla,

CA, USA). Student's *t*-test was used for two-group comparisons. Chi-square test was used for SNP analysis.  $p < 0.05$  was considered as significant for all analyses.

### 3. Results

#### 3.1. Characterization of the Urine-Derived Cells

Many types of cells along the nephron were exfoliated into the urine. Two distinct types of cell colonies were observed. Type I cell colonies were round and small, with a fast growth rate and have clearly defined edges. The cells in the Type I colonies exhibited a dense growth pattern (i, ii of Figure 1A). The cells in the Type II colonies were elongated and less compact than the cells in Type I colonies (iii and iv of Figure 1A). Three cell lines were stained with different proximal tubule cell (PTC) markers. Samples from different salt study participants grew varying amounts of Type I and Type II colonies. In all cell lines there were many CD13- and LTA-positive (PTC makers) immunofluorescent cells [31] (Supplemental Figure S1). There were some of Na<sup>+</sup>-Cl<sup>-</sup> co-transporter (NCC)-positive cells [31] (DCT in one sample, while some Tamm–Horsfall protein (THP)-positive cells [31] (thick ascending limb cells (TAL)) were in another sample (Supplemental Figure S1). There were also L1-CAM-positive cells (CNT) and CD cells marker (Supplemental Figure S1). However, majority were CD13- or LTA-positive cells possibly because of the REBM medium favors the growth of PTC. About 90% of the cells were CD13-positive after AutoMACs sorting (Figure 1B).

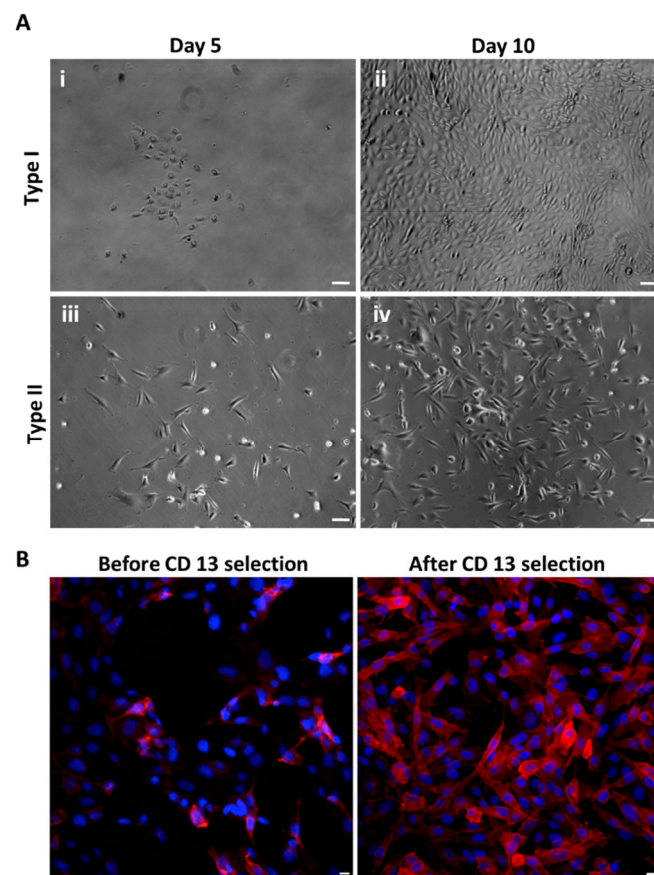


**Figure 1. Urine cell culture.** (A) Representative images of cell colonies from urinary cultures. There are two distinct types of cell colonies. (i,ii) Type I cell colony is commonly found in all the cultures. The round and relatively small cells grow fast with a smooth edge. Within the colony, the cells are compact. (iii,iv): Type II cell colony is less common than type I, but as often found in urine cell culture. The cells were long with slower growth characteristics than type I cells. They formed a loose colony. (Scale bar = 50  $\mu$ m.) (B). Representative images of cells sorted by CD13 in red, a PTC marker. Nuclei were stained blue. (Scale bar = 10  $\mu$ m.)

### 3.2. $\alpha$ ENaC in CD13<sup>+</sup> Urine-Derived Human Renal Tubule Cells (hRTCs)

$\alpha$ ENaC,  $\beta$ ENaC, and  $\gamma$ ENaC were all expressed on the membrane of non-permeabilized primary CD13<sup>+</sup> hRTCs and distributed in a granular pattern throughout the whole cell (Figure 2 Non-permeabilized staining, Supplemental Figure S2 Permeabilized staining). To further confirm if ENaC was present in PTC, human kidney cortical tissue was stained with ENaC antibodies and co-stained with LTA (PTC brush-border marker) or CD13 and the lectin L1-CAM. Both  $\alpha$ ENaC and  $\beta$ ENaC were present in LTA-positive proximal tubule (PT) apical plasma membrane (Figure 3A,B).  $\gamma$ ENaC was evenly distributed only in CD tubules but not PT (Figure 3B), indicating these three subunits of ENaC show different expression patterns in human kidney tissue. Similar staining patterns were confirmed by another set of  $\alpha$ ENaC,  $\beta$ ENaC and  $\gamma$ ENaC antibodies (Supplemental Figure S3). Furthermore, in the CD13<sup>+</sup> primary cells isolated from fresh kidney cortical tissue there was also abundant  $\alpha$ ENaC staining on the apical side of the CD13-positive cells (Supplemental Figure S4).

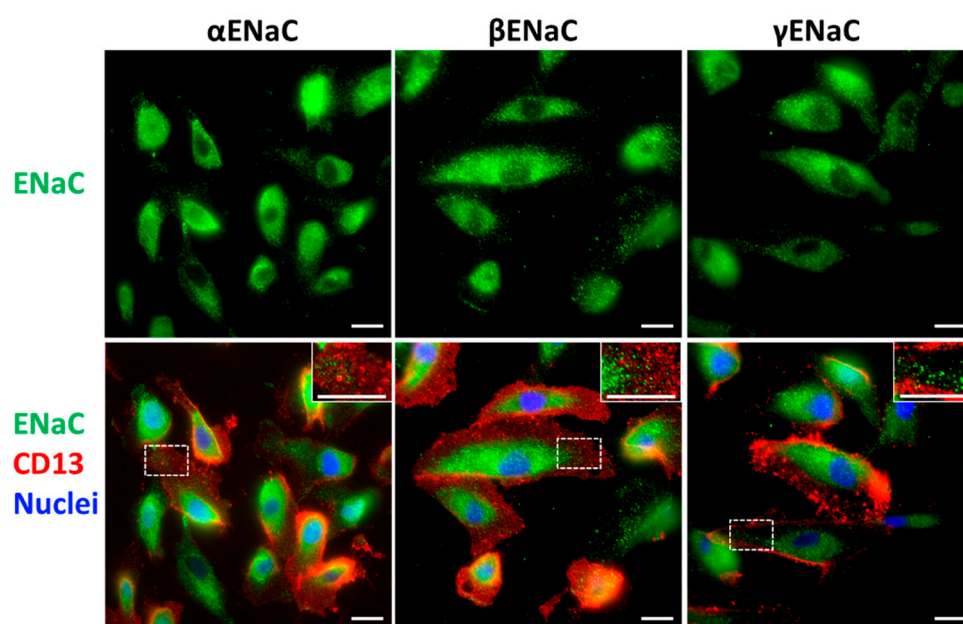


**Figure 2.**  $\alpha$ ENaC,  $\beta$ ENaC, and  $\gamma$ ENaC were stained in non-permeabilized primary urine-derived hRTC.  $\alpha$ ENaC,  $\beta$ ENaC, and  $\gamma$ ENaC were stained green. CD13 staining (red fluorescence) was seen on cell membrane as a punctate pattern. Nuclei were in blue. The detailed view was highlighted by dashed rectangle. (Scale bar = 10  $\mu$ m).

### 3.3. Comparison of $\alpha$ ENaC Expression in Salt Resistant (SR) and Inverse Salt Sensitive (ISS) Urine-Derived hRTCs

To determine whether ENaC was present in hRTCs obtained from individuals with different salt sensitivity phenotypes, western blot analysis was conducted in urine-derived hRTCs from SR, ISS, and SS subjects (regular cell culture medium, 142 mM Na<sup>+</sup>). To confirm the expression of  $\alpha$ ENaC in urine-derived hRTCs,  $\alpha$ ENaC expression was knocked down by siRNA in 3 SR and 3 ISS cell lines. Western blot analysis confirmed that a single band of human  $\alpha$ ENaC with apparent molecular size between 75 and 100 kDa was present in all cell lines and reduced in the knockdown cells (Figure 4A). Figure 4B,C and Supplemental Figure S5A show that the expression of  $\alpha$ ENaC was significantly reduced in ISS cells compared with SR and SS cells (ISS  $0.61 \pm 0.1$ ; SR  $1.31 \pm 0.16$ ; SS  $1.36 \pm 0.25$ ;  $n = 8$ /group, ISS vs. SR, ISS vs. SS  $p < 0.05$ , one-way ANOVA, Tukey's post hoc test, normalized by  $\beta$ -actin, then by SR1).  $\beta$ ENaC appeared as a band with expected molecular weight between 75 and 100 kDa, while  $\gamma$ ENaC appeared as two bands between 75 and 100 kDa (Supplemental Figure S5).  $\beta$ ENaC expression was not different among ISS, SR, and SS (Supplemental Figure S6A,B), while  $\gamma$ ENaC expression was greater in SS than either SR or ISS cells (Supplemental Figure S6C,D).

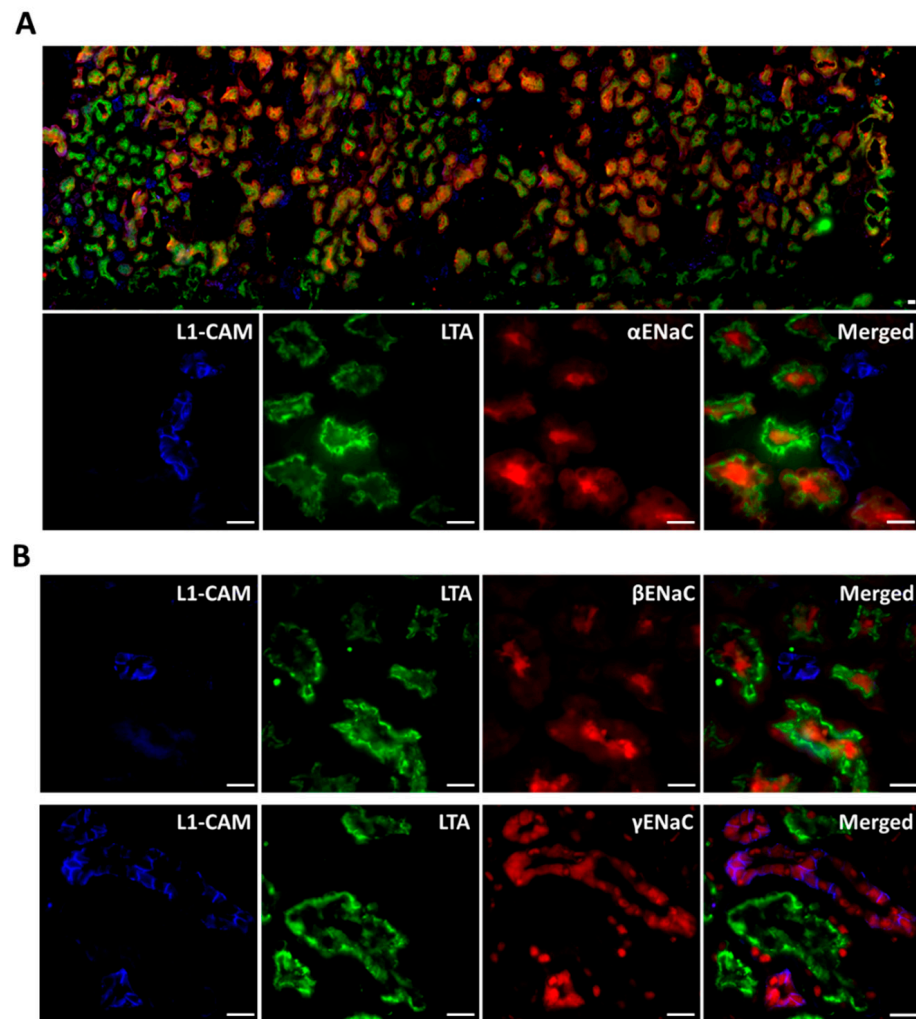


**Figure 3.**  $\alpha$ ENaC,  $\beta$ ENaC, and  $\gamma$ ENaC staining in human renal cortex. (A) The upper panel was a montage showing the overall  $\alpha$ ENaC, L1-CAM, and LTA staining in the whole slice of the tissue; the lower panel showed the close-up images. (B) Representative image of  $\beta$ ENaC and  $\gamma$ ENaC staining in kidney tissue.  $\alpha$ ,  $\beta$ , and  $\gamma$ ENaC were stained in red. LTA was a PTC marker in green. L1-CAM, a CD marker, was in blue. (Scale bar = 10  $\mu$ m).

We further examined potential changes of  $\alpha$ ENaC expression in response to low, normal and high concentrations of  $\text{Na}^+$ . SR and ISS cells were treated overnight with 92 mM  $\text{Na}^+$ , 142 mM  $\text{Na}^+$ , and 192 mM  $\text{Na}^+$ , representing low, normal, and high salt concentrations, respectively. These concentrations were selected because when we measured sodium transport in our PTC cells, we found a linear increase in  $\text{Na}^+$  transport through this concentration range. High-salt treatment increased  $\alpha$ ENaC expression in SR cells (192 mM/142 mM =  $1.22 \pm 0.15 > 1$ ), but decreased it in ISS cells (192 mM/142 mM =  $0.82 \pm 0.09 < 1$ ; SR vs. ISS  $n = 6/\text{group}$ , two-way ANOVA, Sidak's post hoc test,  $p < 0.05$ ) (Figure 4D,E), indicating that high salt concentration may decrease  $\alpha$ ENaC expression in order to reduce salt reabsorption in ISS cells.

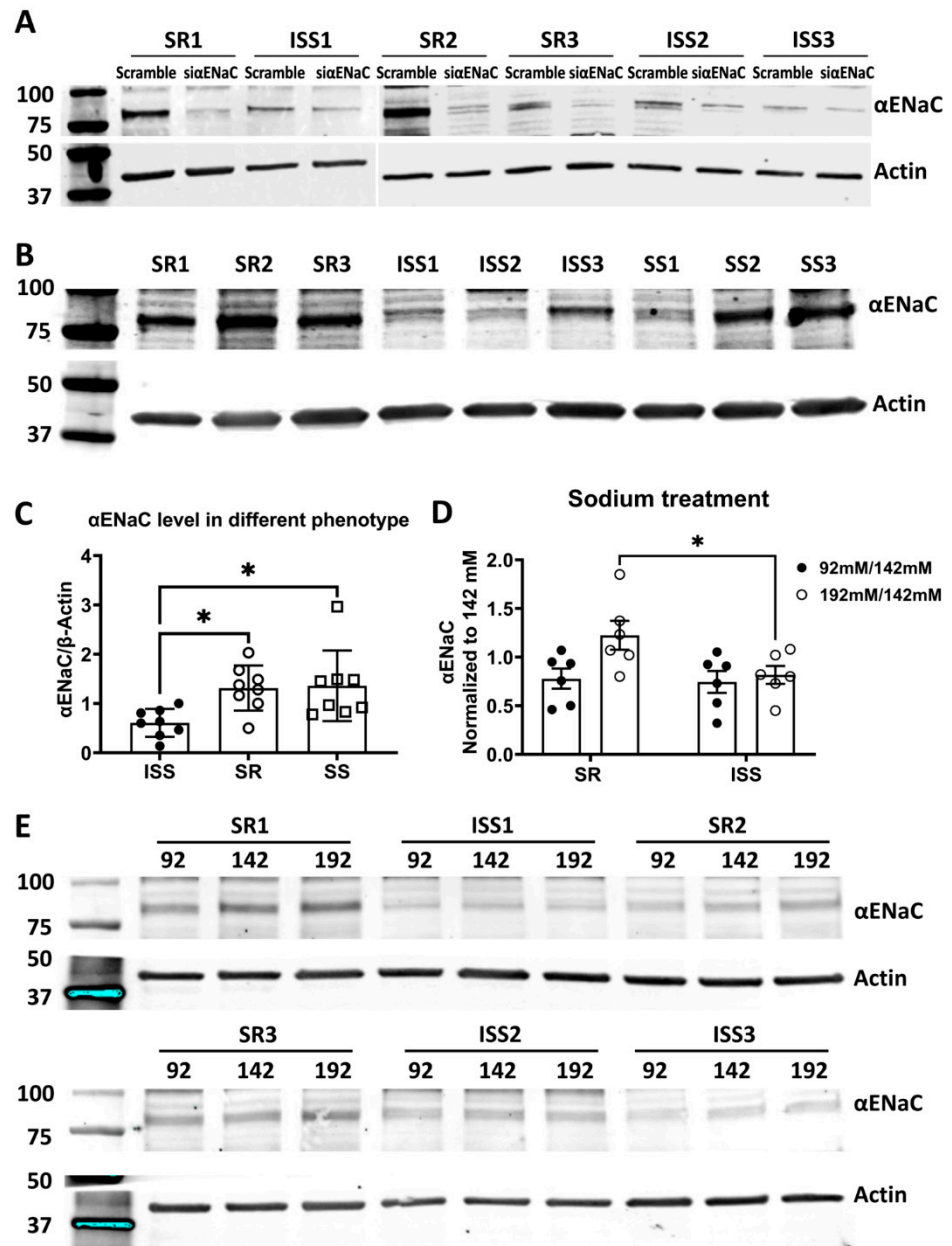


**Figure 4.**  $\alpha$ ENaC in urine-derived renal tubule cells by Western blot. (A)  $\alpha$ ENaC siRNA was used to knock down  $\alpha$ ENaC to confirm that  $\alpha$ ENaC is about 85 kDa. Scrambled RNA was used as control. (B,C) Representative  $\alpha$ ENaC Western blot in urine-derived hRTCs ( $0.61 \pm 0.1$ ; SR  $1.31 \pm 0.16$ ; SS  $1.36 \pm 0.25$ ;  $n = 8$ /group, ISS vs. SR, ISS vs. SS,  $* p < 0.05$ , one-way ANOVA, Tukey’s post hoc test, normalized by  $\beta$ -actin, then by SR1). (D,E) Sodium treatment in SR and ISS CD13+ renal tubule cells. The ratio of high sodium over normal sodium is significantly lower in ISS than SR (192 mM/142 mM: SR,  $1.22 \pm 0.15$  vs. ISS,  $0.82 \pm 0.09$ , two-way ANOVA, Sidak’s post hoc,  $* p < 0.05$ ; 92 mM/142 mM: SR,  $0.78 \pm 0.10$ ; ISS  $0.74 \pm 0.11$ ,  $n = 6$ /group).  $\beta$ -actin was used as loading control in all western blot analysis.

### 3.4. Electrical Activity of ENaC in SR and ISS Urine-Derived Cells

The activity of single ENaC channel in the plasma membrane of urine-derived hRTCs was measured with the cell-attached configuration of the patch-clamp technique. The ENaC-like channels had a similar conductance in SR and ISS cells ( $10.5 \pm 0.7$  pS and  $E_{rev} = 34.1 \pm 1.5$  mV in SR cell and  $10.3 \pm 0.8$  pS and  $E_{rev} = 33.6 \pm 5.5$  mV in ISS cells, Figure 5E). In patch-clamp studies it is common practice to induce the activity of ENaC

currents, serine protease trypsin (5  $\mu\text{g}/\text{mL}$ ) [32,33], a known ENaC activator, was added to the pipette solution (Figure 5A). It should be noticed that the basal ENaC-like channel activity in ISS cells was too low to be recorded without trypsin in the pipette ( $P_o$  = open probability) compared with that in SR cells (Figure 5B). In another set of experiments, we tested the conductivity of the channels when  $\text{Na}^+$  was the main cation in the pipette solution vs.  $\text{Li}^+$ . The current-voltage dependency (IV) showed lower single channel conductance of ENaC-like channels in SR cells with  $\text{Na}^+$  in the pipette solution compared to  $\text{Li}^+$  (from 10.5 down to 8.8 pS, Figure 5C; data obtained in independent experiments); this response is typical for ENaC. Biophysical characteristics of the obtained recordings (reversal potential, conductance) were typical for ENaC-like channels which are well-established in the literature [1,34–36] and did not differ between SR and ISS cells (Figure 5D,E). In both cell lines, trypsin (a protease present in the urine which is known to activate ENaC) in the patch pipette evoked an increase in single ENaC-like channel activity as measured by  $P_o$  [37]. However, the  $P_o$  and the number of active channels in SR and ISS cells were significantly different (Figure 6). ISS cells had higher  $P_o$  than SR cells in response to trypsin both immediately (0 min) and after 4 min of activation (Figure 6C), even though the number of channels recorded at 4 min after GigaOhm seal formation was lower in the ISS than SR cells ( $4.7 \pm 1.7$  vs.  $1.75 \pm 0.5$ ,  $p < 0.05$  in SR vs. ISS lines,  $t$ -test).

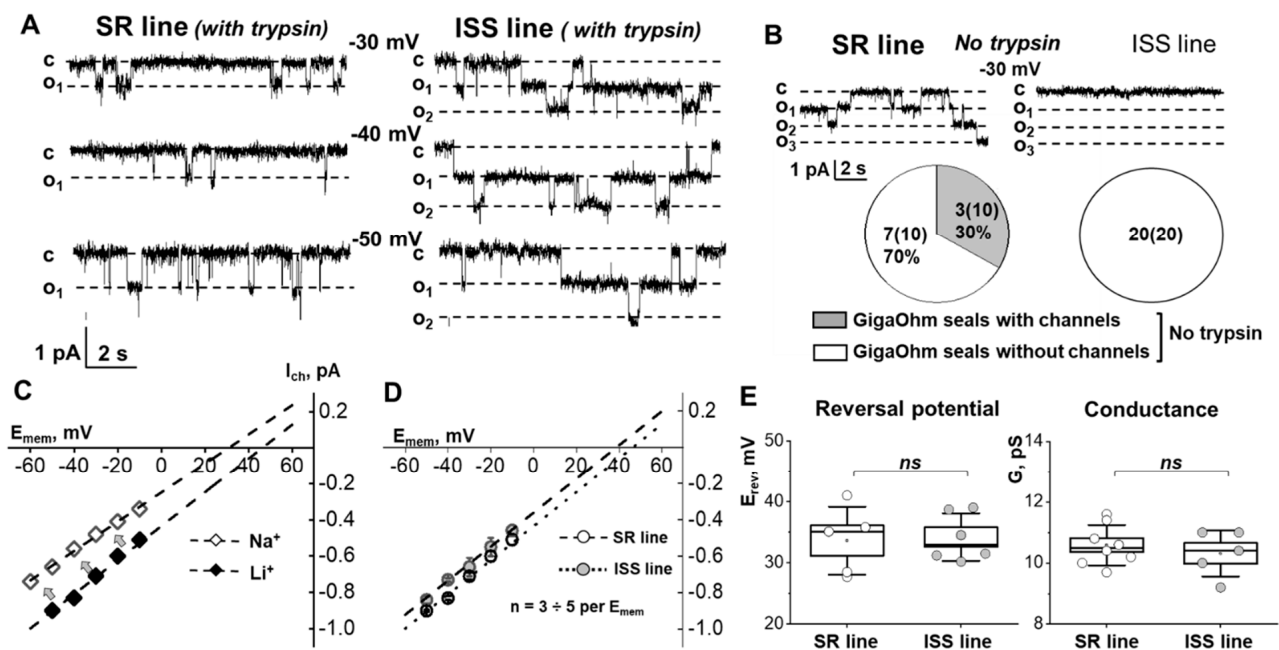


**Figure 5.** ENaC-like channels recorded in SR and ISS cell lines. (A) Representative current traces showing single ENaC-like channels' activity in SR and ISS cell lines recorded at different membrane potentials using patch-clamp electrophysiology. (B) Channel prevalence in successful GigaOhm seals in SR and ISS cell lines without stimulation with trypsin. Representative current traces are shown at  $-30$  mV. (C) IV curve demonstrating lower single channel conductance of ENaC-like channels in a SR cell line with  $\text{Na}^+$  as main cation in the pipette vs.  $\text{Li}^+$ . (D) Cumulative IV curves for single ENaC-like channels recorded in SR and ISS cell lines. (E) Summary graphs demonstrating reversal potential and single channel conductance (SR line:  $E_{rev} = 34.1 \pm 1.5$  mV,  $n = 4$ , and  $10.5 \pm 0.7$  pS  $n = 8$  vs. ISS line:  $E_{rev} = 33.6 \pm 5.5$  mV,  $n = 6$ , and  $10.3 \pm 0.8$  pS,  $n = 5$ ,  $t$ -test).

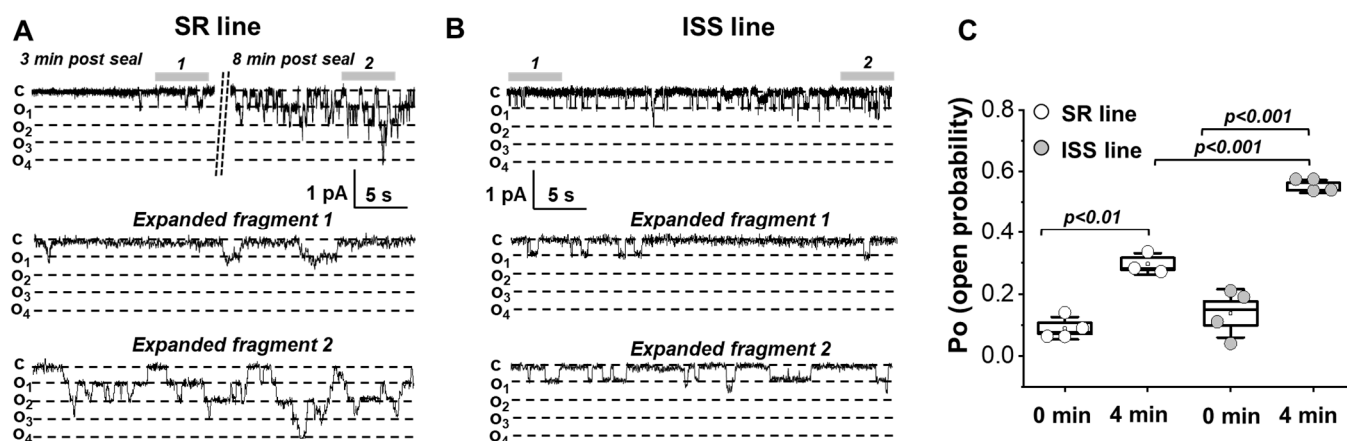


**Figure 6.** Trypsin-triggered activation of ENaC-like channels in the SR and ISS cells. Representative current traces showing single ENaC-like channel activity in SR (A) and ISS (B) cell recorded 1 min after GigaOhm seal formation, and 3 min and 8 min post-seal formation; pipette solution contained 2  $\mu\text{g}/\text{mL}$  trypsin. Shown are representative recordings as well as expanded regions at  $-20$  mV and  $-30$  mV for SR and ISS lines, respectively. Scale bar is noted on the graph, c and oi denote closed and open states (inward currents are downward). (C) A summary graph of the open probability of the channels calculated for at least 20 s recordings immediately after the start of the activation of channels (0 min), and 4 min post-activation start (4 min) (SR: 0 min,  $0.089 \pm 0.018$   $n = 4$  vs. 4 min,  $0.297 \pm 0.02$   $n = 3$ ,  $p < 0.01$ ; ISS: 0 min,  $0.138 \pm 0.039$   $n = 4$  vs. 4 min,  $0.551 \pm 0.012$   $n = 3$ ,  $p < 0.001$ , two-way ANOVA, Tukey's multiple comparisons test).

### 3.5. Aldosterone and $\alpha\text{ENaC}$

In our salt sensitivity studies [24] plasma aldosterone level was significantly higher under low-salt diet (10 mEq NaCl diet) than high-salt diet (300 mEq NaCl diet) in all of ISS, SR, and SS subjects (Figure 7A). ISS subjects tended to have the highest aldosterone level when on the low-salt diet, however, the values were not significantly different from those of SR or SS. The mineralocorticoid receptor (MR) expression was significantly increased to a similar extent by low  $\text{Na}^+$  treatment in both SR and ISS cells through imaging analysis (SR, 92 mM  $12,194 \pm 183$  vs. 142 mM  $10,708 \pm 129$ ; ISS, 92 mM  $12,072 \pm 112$  vs. 142 mM  $11,309 \pm 277$ ;  $n = 4/\text{group}$ ,  $p < 0.01$ , two-way ANOVA, Dunnett's post hoc test) (Figure 7B), indicating that aldosterone may increase MR expression under low-salt diet. High  $\text{Na}^+$  treatment decreased MR expression in ISS but not in SR cells (ISS: 142 mM  $11,309 \pm 277$  vs. 192 mM  $10,425 \pm 52$ ;  $p < 0.01$ ,  $n = 4/\text{group}$ , two-way ANOVA, Dunnett's post hoc test) (Figure 7B). Moreover, PRA was also significantly increased under a low-salt diet, and SS PRA was significantly lower than SR (Figure 8). We then determined if the urine-derived hRTCs would demonstrate the expected aldosterone-stimulated increase in ENaC when incubated under low salt (92 mM  $\text{Na}^+$ ) [38]. After an overnight treatment of the hRTCs with 1  $\mu\text{M}$  aldosterone, MR and  $\alpha\text{ENaC}$  expressions were increased in ISS cells but not in SR cells through imaging analysis (MR: ISS VEH  $11,818 \pm 197$  vs. ISS Aldosterone  $12,835 \pm 178$ ,  $n = 9/\text{group}$ ,  $p < 0.05$ ;  $\alpha\text{ENaC}$ : ISS VEH  $4561 \pm 68$  vs. ISS Aldosterone  $4834 \pm 52$ ,  $n = 9/\text{group}$ ,  $p < 0.01$ , two-way ANOVA, Sidak's post hoc test) (Figure 7C,D, Supplemental Figure S7).

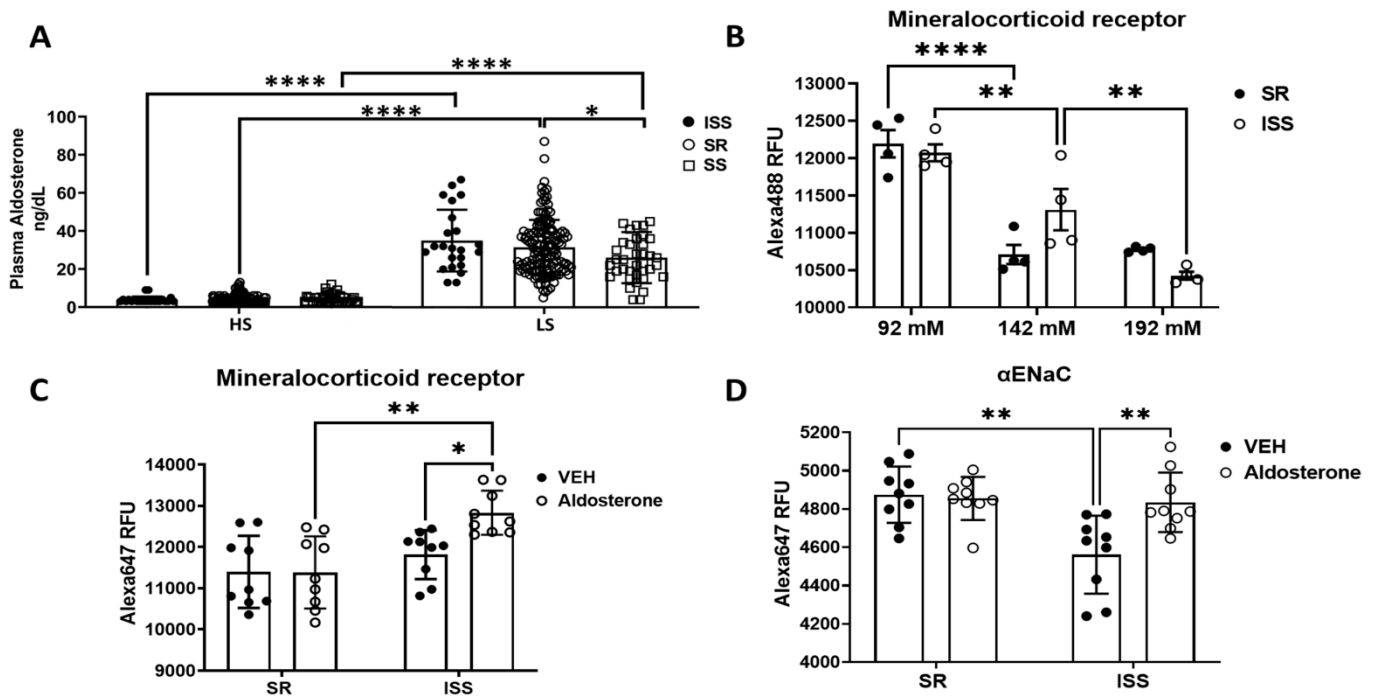


**Figure 7.** Aldosterone level from our dietary salt study and aldosterone treatment on urine-derived renal tubule cells. (A) Plasma aldosterone level of ISS, SR and SS participants on low- and high-salt diets (ISS HS,  $3.8 \pm 0.38$ ,  $n = 26$ ; ISS LS,  $35 \pm 3.38$ ,  $n = 22$ ; SR HS,  $4.34 \pm 0.18$ ,  $n = 180$ ; SR LS,  $32.62 \pm 1.6$ ,  $n = 152$ ; SS HS,  $4.65 \pm 0.35$ ,  $n = 43$ ; SS LS,  $26.08 \pm 2.18$ ,  $n = 38$ ; HS vs. LS,  $p < 0.001$ , two-way ANOVA, Tukey’s multiple comparisons test). (B) MR level under different sodium treatments in both SR and ISS cells (SR, 92 mM  $12,194 \pm 183$  vs. 142 mM  $10,708 \pm 129$ ; ISS, 92 mM  $12,072 \pm 112$  vs. 142 mM  $11,309 \pm 277$ ;  $n = 4$ /group,  $p < 0.01$ , two-way ANOVA, Dunnett’s multiple comparisons test). (C,D) Mineralocorticoid receptor (MR) and  $\alpha$ ENaC level under aldosterone treatment ( $1 \mu\text{M}$ ) on both SR and ISS cells (MR: ISS VEH  $11,818 \pm 197$  vs. ISS Aldosterone  $12,835 \pm 178$ ,  $n = 9$ /group,  $p < 0.05$ ;  $\alpha$ ENaC: ISS VEH  $4561 \pm 68$  vs. ISS Aldosterone  $4834 \pm 52$ ,  $n = 9$ /group,  $p < 0.01$ , two-way ANOVA, Tukey’s multiple comparisons test). \*  $p < 0.05$ , \*\*  $p < 0.01$ , \*\*\*\*  $p < 0.001$ .

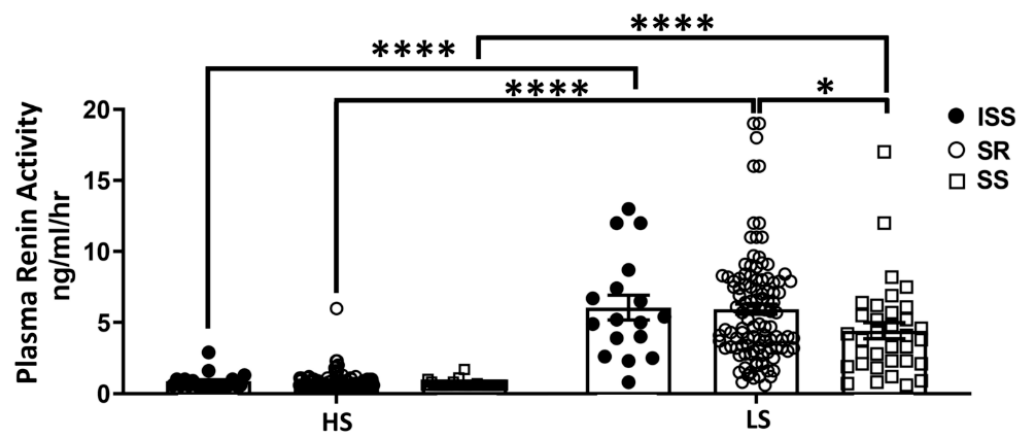


**Figure 8.** Plasma renin activity level of ISS, SR and SS participants on low and high-salt diets (ISS HS,  $0.86 \pm 0.12$ ,  $n = 21$ ; ISS LS,  $6.05 \pm 0.87$ ,  $n = 17$ ; SR HS,  $0.8 \pm 0.55$ ,  $n = 144$ ; SR LS,  $5.94 \pm 0.36$ ,  $n = 108$ ; SS HS,  $0.66 \pm 0.03$ ,  $n = 44$ ; SS LS,  $4.43 \pm 0.57$ ,  $n = 34$ ; HS vs. LS,  $p < 0.001$ , two-way ANOVA, Tukey’s multiple comparisons test). \*  $p < 0.05$ , \*\*\*\*  $p < 0.001$ .

**3.6. Gene Variant rs4764586 of  $\alpha$ ENaC and Inverse Salt Sensitivity**

Gene variants in  $\alpha$ ENaC have been shown to be associated with salt sensitivity of BP [21], and we verified that the specific gene variant rs4764586 is significantly associated

with ISS in our salt study as well ( $\chi^2 = 9.73$ ,  $p < 0.05$ ) (Table 1). However, the other two SNPs, rs11614164 and rs3741914, did not show any difference. In our salt sensitivity clinical study, 13% of participants ( $N = 37/280$ ) had a paradoxical increase in  $\Delta\text{MAP} \geq 7$  mmHg on a low NaCl diet in comparison with a high NaCl diet, defined as ISS, versus SR (64%) and SS (23%). The prevalence of the homozygous minor allele  $\alpha\text{ENaC}$  in the ISS group was higher compared with SR and SS (ISS, 16%; SR, 5%; SS, 11%). The odds ratio of ISS to non-ISS (SR plus SS) was 1.91 indicating the odds were 1.91 times higher for those who have rs4764586 to become ISS compare with those who were homozygous major variant (Supplemental Table S2). Urine-derived hRTCs showed the lowest  $\alpha\text{ENaC}$  protein expression in the rs4764586 homozygous minor variants and the highest in the homozygous major variants (homozygous of major variants,  $1.25 \pm 0.24$ ,  $n = 9$ ; heterozygous,  $1.13 \pm 0.14$ ,  $n = 12$ ; homozygous of minor variants,  $0.47 \pm 0.18$ ,  $n = 3$ , Supplemental Figure S5).

**Table 1.** Distribution of  $\alpha\text{ENaC}$  rare variant, rs4764586, in different salt sensitivities.

Salt Sensitivity	Homozygous of Major Variants	Heterozygous	Homozygous of Minor Variants	Total ( $n = 280$ )
ISS	14 (38%)	17 (46%)	6 (16%)	37 (13%)
SR	93 (52%)	76 (43%)	9 (5%)	178 (64%)
SS	38 (58%)	20 (31%)	7 (11%)	65 (23%)

$\chi^2 = 9.73$   $p < 0.05$ .

#### 4. Discussion

Renal ENaC plays an important role in the regulation of whole-body  $\text{Na}^+$  homeostasis. The ENaC mediated  $\text{Na}^+$  reabsorption occurs predominately in collecting duct because of its abundant expression in that nephron segment. Using urine-derived renal tubule cells (RTC) and human kidney tissue sections, our current studies demonstrate that  $\alpha$ ,  $\beta$ , and  $\gamma\text{ENaC}$  are present in urine-derived RTC, including PTC. The immunostaining was performed by two sets of antibodies, especially the StressMarq antibodies developed by Dr. Mark Knepper [39]. Both  $\alpha$  and  $\beta\text{ENaC}$  were present in PT, and  $\gamma\text{ENaC}$  was present only in CD. It was found that hRTC from ISS individuals were more sensitive to aldosterone induced upregulation of  $\alpha\text{ENaC}$  expression even though the basal levels of  $\alpha\text{ENaC}$  were lower than the hRTC from SR individuals. In addition,  $\alpha\text{ENaC}$  expression in hRTC in response to high-salt treatment was in opposite directions in ISS and SR, e.g., high salt reduced  $\alpha\text{ENaC}$  level in hRTC from ISS but increased  $\alpha\text{ENaC}$  level in the cells from SR. These findings suggest that differential regulation of  $\alpha\text{ENaC}$  expression and function may be one additional mechanism that contributes to inverse salt sensitivity of BP.

RNA-seq data in mouse and rat demonstrate that  $\alpha\text{ENaC}$  is more ubiquitous and plentiful than the other two subunits [39,40]. Even though the  $\alpha\text{ENaC}$  mRNA level is much lower in PT than that in DCT, CNT, or CD, its mRNA can be detected throughout the renal tubules [40,41]. Maximal ENaC activity is dependent on all three subunits being present [42,43].  $\alpha\text{ENaC}$  alone is sufficient to induce a  $\text{Na}^+$  current [1]. Some vascular smooth muscle cells in renal arteries contain only  $\beta$  and  $\gamma$  ENaC, but not the  $\alpha$  isoform.  $\alpha\text{ENaC}$  plays an important role in pressure-induced vasoconstriction [44]. Moreover,  $\beta\text{ENaC}$  alone has been shown to control renal arterial myogenic tone both in vitro and in vivo [45,46]. In *Xenopus*,  $\alpha$ ,  $\beta$ , and  $\delta$  ENaC can form homomeric functional channels that show amiloride sensitive currents, and channels containing two subunits also respond to shear force [47]. Therefore, our novel finding that  $\alpha$  and  $\beta$  ENaC may form a functional ENaC-like channel in renal proximal tubule cells is consistent with the pleotropic role of ENaC in renal sodium homeostasis.

Differential regulation of sodium balance contributes to an individual's "personal salt index" [27]. Inverse salt sensitivity is characterized by lower MAP while consuming the high-sodium diet and an elevated MAP while consuming the low-sodium diet. Research has shown that both high and low sodium diets result in increased cardiovascular morbidity

and mortality, and is referred to a “J”-shaped relationship [48–50]. However, the etiology of the harmful effect of low sodium has not been determined. We found that expression of  $\alpha$ ENaC protein in the urine-derived renal cells was significantly lower in ISS than in SR. Sodium treatment increased  $\alpha$ ENaC in SR but decreased it in ISS under 192 mM sodium. These findings indicate that the ISS with lower BP on high-salt diet may result from reduced sodium reabsorption because of less  $\alpha$ ENaC expression. Interestingly, reduction in  $\alpha$ ENaC was also observed in rats on  $\text{Na}^+$ -replete diet compared with the rats on low- $\text{Na}^+$  diet [51]. Single-channel patch clamp analysis showed that ISS cells have higher open probability of ENaC-like currents post-trypsin treatment compared with SR cells. These changes indicate that ISS cells not only have reduced levels of total  $\alpha$ ENaC but also have more silent ENaC-like channels in the membrane.

Aldosterone is dramatically increased under low salt conditions [52]. It also increases ENaC abundance and stimulates ENaC activity at the apical cell membrane through mineralocorticoid receptor (MR) and an ENaC-regulatory-complex pathway with involvement of SGK1 (serum and glucocorticoid-induced kinase 1) and GILZ (glucocorticoid-induced leucine zipper protein) [53]. In our clinical study, as anticipated, plasma aldosterone increased under low sodium diet in all participants. There was a trend that ISS individuals had higher plasma aldosterone concentrations. The *in vitro* study showed that aldosterone treatment upregulated MR and  $\alpha$ ENaC in PTC from ISS individuals but not from SR individuals. This could explain how low-sodium-diet-induced elevation of aldosterone causes a more dramatic increase in both MR and ENaC expression in ISS cells which leads to more efficient sodium reabsorption and increased BP. By contrast, under high salt conditions ISS individuals are protected from increased BP by lower ENaC expression and greater natriuresis. The fact that aldosterone was not significantly different when comparing ISS to SR under high-salt diet indicate that these particular experiments may have been underpowered, since ISS occurs at a lower frequency (13%) compared with SS (23%). Follow up studies will be necessary to answer this particular question. The elevated circulating aldosterone in ISS while consuming a low-salt diet coupled with the higher sensitivity to aldosterone in ISS *ex-vivo* urine-derived renal cells may be a diagnostic tool to identify ISS individuals. We also found an elevated PRA levels while on the low-salt diet, and SS individuals showed significantly lower PRA than SR individuals, indicating that low-salt diet is protective for SS individuals.

$\alpha$ ENaC variants were reported to be associated with salt sensitivity of BP in a Chinese GenSalt study [21]. Those who carried variant rs4764586 had 1.36-fold increased odds ratio for salt sensitivity [21]. In our study where we defined  $\Delta\text{MAP} \leq -7$  mmHg as ISS, rs4764586 was also associated with salt sensitivity. However, this rare variant shows increased odd ratio (1.91) in ISS, indicating that this rare variant may be associated with inverse salt sensitivity of BP as well.

Others have also demonstrated the utility of urine-derived cells. For example, the first successful culture of exfoliated urinary cells was from newborn infants reported by Sutherland and Bain [54], and subsequently multiple groups have reproduced the culture from both infant and adult urine [55–59]. These urine-derived cells were characterized as a heterogeneous population of different cell types, including urothelial, PT, DCT, and fibroblast-like cells [59,60]. More recently, a subpopulation of urine-derived cells was also identified as a good source of stem cells for cell therapy and tissue engineering [61–64]. All of the previous studies were performed on the primary cell culture. In our culture technique, the cells are immortalized by *tert* and can be sub-cultured as a stable cell line for many passages. Consistent with the previous reports [56–59], there were two cell types in most cultures and the type I cell colony with smooth edge usually grows rapidly and is easy to maintain as a cell line. In our study, we also found that there were different types of renal tubule cells, such as DCT, CD, etc. Urine-derived renal tubule cells can serve as representative models to study human renal cell physiology.

A limitation of our studies is that we did not determine the effect of high and low-salt diets on ENaC expression and activity in renal tissue. Renal tissue cannot be obtained from

normal individuals as IRB approval cannot be obtained for experimental renal biopsies. Discard kidneys from transplant services have proved not to exhibit normal physiological responses related to  $\text{Na}^+$  homeostasis and also exhibit necrotic features. Another limitation is the sample size of urine cell lines, which is dependent on participant recruitment and urine cell culture. Furthermore, characterization of these urine-derived renal tubule cells should be performed in later passages because the cells have stem-cell characteristics and may de-differentiate after being subcultured many times [65]. Physiologic studies in rodents demonstrated that infusion of a relatively large amount of NaCl decreases the expression of ENaC [50]. Future studies of hRTCs from ISS individuals and SR controls obtained from fresh urine might yield some insight into to whether elevated  $\text{Na}^+$  increases or decreases ENaC expression. Further, the differential regulation of ENaC between ISS and SR also need to be further addressed. For example, Mammalian Ste20 kinase 3 (MST3) may be involved in regulating ENaC expression in these hRTCs, which maintain BP through inhibiting ENaC expression in mice [66,67].

**Supplementary Materials:** The following supporting information can be downloaded at: <https://www.mdpi.com/article/10.3390/biomedicines10050981/s1>, Figure S1: Representative images show different types of renal cells in the urine; Figure S2:  $\alpha$ ENaC,  $\beta$ ENaC and  $\gamma$ ENaC staining in permeabilized urine-derived renaltubule cells; Figure S3:  $\alpha$ ENaC,  $\beta$ ENaC and  $\gamma$ ENaC (StressMarq antibodies) staining in human renal cortex; Figure S4:  $\alpha$ ENaC was stained in cells digested from fresh human renal cortex in suspension; Figure S5  $\alpha$ ENaC western blot analysis in more urine-derived hRTCs; Figure S6:  $\beta$ ENaC and  $\gamma$ ENaC are found in CD13+ renal tubule cells; Figure S7: Representative images of mineralocorticoid receptor (MR) and  $\alpha$ ENaC immunostaining under aldosterone treatment; Table S1: Characteristics of UVA Study Subjects (Mean  $\pm$  SD); Table S2: Odds Ratio.

**Author Contributions:** P.X. performed and designed most experiments and statistical analysis, interpreted them, and wrote the manuscript. A.V.S. and D.V.I. performed patch clamp and statistical analysis, interpreted the results, and reviewed the manuscript. J.J.G. provided ideas, interpreted the results, reviewed the manuscript, and supervised the whole project. M.A. and R.M.C. provided clinical samples and aldosterone data and reviewed the manuscript. W.Y. and P.A.J. reviewed and edited the manuscript. R.A.F. interpreted experiments, reviewed and edited the manuscript, and supervised the whole project as principal investigator. All authors have read and agreed to the published version of the manuscript.

**Funding:** These studies were funded by P01HL074940 and R00 DK105160, R01HL148114, R01DK119652, 2-R01-HL-128189, Dialysis Clinic Inc Reserve Fund, the APS Research Career Enhancement, and Lazaro J Madel awards.

**Institutional Review Board Statement:** The study was conducted in accordance with the Declaration of Helsinki, and approved by the Institutional Review Board of University of Virginia (protocol code HSR# 13310, 10/11/2021 and HSR # 11494, 6/17/2021).

**Informed Consent Statement:** Informed consent was obtained from all subjects involved in the study.

**Data Availability Statement:** Not applicable.

**Acknowledgments:** We thank Stephen Marshall, Katie Schiermeyer, and Qing Zhang for their support and helpful discussions during the performance of these studies.

**Conflicts of Interest:** The authors declare no conflict of interest.

## Nonstandard Abbreviations and Acronyms

BP	blood pressure
CD	collecting duct
CDC	collecting duct cell
CNT	connecting tubule
DCT	distal convoluted tubule
DTC	distal tubule cell

ENaC	epithelial sodium channel
hRTC	human renal tubular epithelial cell
tert	telomerase reverse transcriptase
ISS	inverse salt sensitive
KO	knockout
MAP	mean arterial pressure
NCC	Na <sup>+</sup> -Cl <sup>-</sup> co-transporter
PT	proximal tubule
PTC	proximal tubule cell
SR	salt resistant
SS	salt sensitivity
TAL	thick ascending limb
THP	Tamm-Horsfall protein

## References

- Canessa, C.M.; Schild, L.; Buell, G.; Thorens, B.; Gautschi, I.; Horisberger, J.D.; Rossier, B.C. Amiloride-sensitive epithelial Na<sup>+</sup> channel is made of three homologous subunits. *Nature* **1994**, *367*, 463–467. [[CrossRef](#)] [[PubMed](#)]
- Kleyman, T.R.; Eaton, D.C. Regulating ENaC's gate. *Am. J. Physiol. Cell Physiol.* **2020**, *318*, C150–C162. [[CrossRef](#)] [[PubMed](#)]
- Kashlan, O.B.; Adelman, J.L.; Okumura, S.; Blobner, B.M.; Zuzek, Z.; Hughey, R.P.; Kleyman, T.R.; Grabe, M. Constraint-based, homology model of the extracellular domain of the epithelial Na<sup>+</sup> channel  $\alpha$  subunit reveals a mechanism of channel activation by proteases. *J. Biol. Chem.* **2011**, *286*, 649–660. [[CrossRef](#)] [[PubMed](#)]
- Kellenberger, S.; Schild, L. International union of basic and clinical pharmacology. Xci. Structure, function, and pharmacology of acid-sensing ion channels and the epithelial Na<sup>+</sup> channel. *Pharmacol. Rev.* **2015**, *67*, 1–35. [[CrossRef](#)]
- Staruschenko, A.; Adams, E.; Booth, R.E.; Stockand, J.D. Epithelial Na<sup>+</sup> channel subunit stoichiometry. *Biophys. J.* **2005**, *88*, 3966–3975. [[CrossRef](#)]
- Stockand, J.D.; Staruschenko, A.; Pochynyuk, O.; Booth, R.E.; Silverthorn, D.U. Insight toward epithelial Na<sup>+</sup> channel mechanism revealed by the acid-sensing ion channel 1 structure. *IUBMB Life* **2008**, *60*, 620–628. [[CrossRef](#)]
- Noreng, S.; Bharadwaj, A.; Posert, R.; Yoshioka, C.; Bacongus, I. Structure of the human epithelial sodium channel by cryo-electron microscopy. *eLife* **2018**, *7*, e39340. [[CrossRef](#)]
- Loffing, J.; Kaissling, B. Sodium and calcium transport pathways along the mammalian distal nephron: From rabbit to human. *Am. J. Physiol. Ren. Physiol.* **2003**, *284*, F628–F643. [[CrossRef](#)]
- Rossier, B.C. Epithelial sodium channel (ENaC) and the control of blood pressure. *Curr. Opin. Pharmacol.* **2014**, *15*, 33–46. [[CrossRef](#)]
- Bens, M.; Vallet, V.; Cluzeaud, F.; Pascual-Letallec, L.; Kahn, A.; Rafestin-Oblin, M.E.; Rossier, B.C.; Vandewalle, A. Corticosteroid-dependent sodium transport in a novel immortalized mouse collecting duct principal cell line. *J. Am. Soc. Nephrol.* **1999**, *10*, 923–934. [[CrossRef](#)]
- Alvarez de la Rosa, D.; Canessa, C.M. Role of SGK in hormonal regulation of epithelial sodium channel in A6 cells. *Am. J. Physiol. Cell Physiol.* **2003**, *284*, C404–C414. [[CrossRef](#)] [[PubMed](#)]
- Strautnieks, S.S.; Thompson, R.J.; Hanukoglu, A.; Dillon, M.J.; Hanukoglu, I.; Kuhnle, U.; Seckl, J.; Gardiner, R.M.; Chung, E. Localisation of pseudohypoaldosteronism genes to chromosome 16p12.2-13.11 and 12p13.1-pter by homozygosity mapping. *Hum. Mol. Genet.* **1996**, *5*, 293–299. [[CrossRef](#)] [[PubMed](#)]
- Chang, S.S.; Grunder, S.; Hanukoglu, A.; Rösler, A.; Mathew, P.M.; Hanukoglu, I.; Schild, L.; Lu, Y.; Shimkets, R.A.; Nelson-Williams, C.; et al. Mutations in subunits of the epithelial sodium channel cause salt wasting with hyperkalaemic acidosis, pseudohypoaldosteronism type 1. *Nat. Genet.* **1996**, *12*, 248–253. [[CrossRef](#)]
- Rossier, B.C.; Pradervand, S.; Schild, L.; Hummler, E. Epithelial sodium channel and the control of sodium balance: Interaction between genetic and environmental factors. *Annu. Rev. Physiol.* **2002**, *64*, 877–897. [[CrossRef](#)]
- Edelheit, O.; Hanukoglu, I.; Gizewska, M.; Kandemir, N.; Tenenbaum-Rakover, Y.; Yurdakök, M.; Zajacsek, S.; Hanukoglu, A. Novel mutations in epithelial sodium channel (ENaC) subunit genes and phenotypic expression of multisystem pseudohypoaldosteronism. *Clin. Endocrinol.* **2005**, *6*, 547–553. [[CrossRef](#)]
- Hummler, E.; Barker, P.; Gatzky, J.; Beermann, F.; Verdumo, C.; Schmidt, A.; Boucher, R.; Rossier, B.C. Early death due to defective neonatal lung liquid clearance in alpha-ENaC-deficient mice. *Nat. Genet.* **1996**, *12*, 325–328. [[CrossRef](#)] [[PubMed](#)]
- Barker, P.M.; Nguyen, M.S.; Gatzky, J.T.; Grubb, B.; Norman, H.; Hummler, E.; Rossier, B.; Boucher, R.C.; Koller, B. Role of gammaENaC subunit in lung liquid clearance and electrolyte balance in newborn mice. Insights into perinatal adaptation and pseudohypoaldosteronism. *J. Clin. Investig.* **1998**, *102*, 1634–1640. [[CrossRef](#)]
- McDonald, F.J.; Yang, B.; Hrstka, R.F.; Drummond, H.A.; Tarr, D.E.; McCray, P.B., Jr.; Stokes, J.B.; Welsh, M.J.; Williamson, R.A. Disruption of the beta subunit of the epithelial Na<sup>+</sup> channel in mice: Hyperkalemia and neonatal death associated with a pseudohypoaldosteronism phenotype. *Proc. Natl. Acad. Sci. USA* **1999**, *96*, 1727–1731. [[CrossRef](#)]

19. Rubera, I.; Loffing, J.; Palmer, L.G.; Frindt, G.; Fowler-Jaeger, N.; Sauter, D.; Carroll, T.; McMahon, A.; Hummler, E.; Rossier, B.C. Collecting duct-specific gene inactivation of alpha enac in the mouse kidney does not impair sodium and potassium balance. *J. Clin. Investig.* **2003**, *112*, 554–565. [[CrossRef](#)]
20. Christensen, B.M.; Perrier, R.; Wang, Q.; Zuber, A.M.; Maillard, M.; Mordasini, D.; Malsure, S.; Ronzaud, C.; Stehle, J.C.; Rossier, B.C.; et al. Sodium and potassium balance depends on  $\alpha$ ENaC expression in connecting tubule. *J. Am. Soc. Nephrol.* **2010**, *21*, 1942–1951. [[CrossRef](#)]
21. Gu, X.; Gu, D.; He, J.; Rao, D.C.; Hixson, J.E.; Chen, J.; Li, J.; Huang, J.; Wu, X.; Rice, T.K.; et al. Resequencing epithelial sodium channel genes identifies rare variants associated with blood pressure salt-sensitivity: The GenSalt study. *Am. J. Hypertens.* **2018**, *31*, 205–211. [[CrossRef](#)] [[PubMed](#)]
22. Weinberger, M.H.; Fineberg, N.S.; Fineberg, S.E.; Weinberger, M. Salt sensitivity, pulse pressure, and death in normal and hypertensive humans. *Hypertension* **2001**, *37*, 429–432. [[CrossRef](#)] [[PubMed](#)]
23. Weinberger, M.H. Salt sensitivity is associated with an increased mortality in both normal and hypertensive humans. *J. Clin. Hypertension* **2002**, *4*, 274–276. [[CrossRef](#)] [[PubMed](#)]
24. Carey, R.M.; Schoeffel, C.D.; Gildea, J.J.; Jones, J.E.; McGrath, H.E.; Gordon, L.N.; Park, M.J.; Sobota, R.S.; Underwood, P.C.; Williams, J.; et al. Salt sensitivity of blood pressure is associated with polymorphisms in the sodium-bicarbonate cotransporter. *Hypertension* **2012**, *60*, 1359–1366. [[CrossRef](#)] [[PubMed](#)]
25. Balafa, O.; Kalaitzidis, R.G. Salt sensitivity and hypertension. *J. Hum. Hypertens.* **2020**, *35*, 184–192. [[CrossRef](#)]
26. Felder, R.A.; White, M.J.; Williams, S.M.; Jose, P.A. Diagnostic tools for hypertension and salt sensitivity testing. *Curr. Opin. Nephrol. Hypertens.* **2013**, *22*, 65–76. [[CrossRef](#)]
27. Gildea, J.J.; Xu, P.; Carlson, J.M.; Gaglione, R.T.; Bigler Wang, D.; Kemp, B.A.; Reyes, C.M.; McGrath, H.E.; Carey, R.M.; Jose, P.A.; et al. The sodium-bicarbonate cotransporter NBCe2 (slc4a5) expressed in human renal proximal tubules shows increased apical expression under high-salt conditions. *Am. J. Physiol. Regul. Integr. Comp. Physiol.* **2015**, *309*, R1447–R1459. [[CrossRef](#)]
28. Gildea, J.J.; McGrath, H.E.; Van Sciver, R.E.; Wang, D.B.; Felder, R.A. Isolation, growth, and characterization of human renal epithelial cells using traditional and 3d methods. *Methods Mol. Biol.* **2013**, *945*, 329–345.
29. Gildea, J.J.; Lahiff, D.T.; Van Sciver, R.E.; Weiss, R.S.; Shah, N.; McGrath, H.E.; Schoeffel, C.D.; Jose, P.A.; Carey, R.M.; Felder, R.A. A linear relationship between the ex-vivo sodium mediated expression of two sodium regulatory pathways as a surrogate marker of salt sensitivity of blood pressure in exfoliated human renal proximal tubule cells: The virtual renal biopsy. *Clin. Chim. Acta* **2013**, *421*, 236–242. [[CrossRef](#)]
30. Pavlov, T.S.; Levchenko, V.; Ilatovskaya, D.V.; Moreno, C.; Staruschenko, A. Renal sodium transport in renin-deficient dahl salt-sensitive rats. *J. Renin Angiotensin Aldosterone Syst.* **2016**, *17*, 1470320316653858. [[CrossRef](#)]
31. Gildea, J.J.; Shah, I.; Weiss, R.; Casscells, N.D.; McGrath, H.E.; Zhang, J.; Jones, J.E.; Felder, R.A. HK-2 human renal proximal tubule cells as a model for G protein-coupled receptor kinase type 4-mediated dopamine 1 receptor uncoupling. *Hypertension* **2010**, *56*, 505–511. [[CrossRef](#)] [[PubMed](#)]
32. Nesterov, V.; Dahlmann, A.; Bertog, M.; Korbmacher, C. Trypsin can activate the epithelial sodium channel (ENaC) in microdissected mouse distal nephron. *Am. J. Physiol. Ren. Physiol.* **2008**, *295*, F1052–F1062. [[CrossRef](#)] [[PubMed](#)]
33. Haerteis, S.; Krappitz, A.; Krappitz, M.; Murphy, J.E.; Bertog, M.; Krueger, B.; Nacken, R.; Chung, H.; Hollenberg, M.D.; Knecht, W.; et al. Proteolytic activation of the human epithelial sodium channel by trypsin IV and trypsin I involves distinct cleavage sites. *J. Biol. Chem.* **2014**, *289*, 19067–19078. [[CrossRef](#)] [[PubMed](#)]
34. Kellenberger, S.; Schild, L. Epithelial sodium channel/degenerin family of ion channels: A variety of functions for a shared structure. *Physiol. Rev.* **2002**, *82*, 735–767. [[CrossRef](#)]
35. Diakov, A.; Bera, K.; Mokrushina, M.; Krueger, B.; Korbmacher, C. Cleavage in the  $\gamma$ -subunit of the epithelial sodium channel (ENaC) plays an important role in the proteolytic activation of near-silent channels. *J. Physiol.* **2008**, *586*, 4587–4608. [[CrossRef](#)]
36. Ji, H.L.; Su, X.F.; Kedar, S.; Li, J.; Barbry, P.; Smith, P.R.; Matalon, S.; Benos, D.J. Delta-subunit confers novel biophysical features to alpha beta gamma-human epithelial sodium channel (ENaC) via a physical interaction. *J. Biol. Chem.* **2006**, *281*, 8233–8241. [[CrossRef](#)]
37. Hughey, R.P.; Bruns, J.B.; Kinlough, C.L.; Harkleroad, K.L.; Tong, Q.; Carattino, M.D.; Carattino, M.D.; Johnson, J.P.; Stockand, J.D.; Kleyman, T.R. Epithelial sodium channels are activated by furindependent proteolysis. *J. Biol. Chem.* **2004**, *279*, 18111–18114. [[CrossRef](#)]
38. Swanson, E.A.; Nelson, J.W.; Jeng, S.; Erspamer, K.J.; Yang, C.L.; McWeeney, S.; Ellison, D.H. Salt-sensitive transcriptome of isolated kidney distal tubule cells. *Physiol. Genom.* **2019**, *51*, 125–135. [[CrossRef](#)]
39. Masilamani, S.; Kim, G.H.; Mitchell, C.; Wade, J.B.; Knepper, M.A. Aldosterone-mediated regulation of ENaC alpha, beta, and gamma subunit proteins in rat kidney. *J. Clin. Investig.* **1999**, *104*, R19–R23. [[CrossRef](#)]
40. Lee, J.W.; Chou, C.L.; Knepper, M.A. Deep sequencing in microdissected renal tubules identifies nephron segment-specific transcriptomes. *J. Am. Soc. Nephrol.* **2015**, *26*, 2669–2677. [[CrossRef](#)]
41. Chen, L.; Clark, J.Z.; Nelson, J.W.; Kaissling, B.; Ellison, D.H.; Knepper, M.A. Renal-tubule epithelial cell nomenclature for single-cell rna-sequencing studies. *J. Am. Soc. Nephrol.* **2019**, *30*, 1358–1364. [[CrossRef](#)] [[PubMed](#)]

42. Hanukogluab, A.; Edelheitcf, O.; Shrikiyf, Y.; Gizewska, M.; Dascal, N.; Hanukoglu, I. Renin–aldosterone response, urinary Na/K ratio and growth in pseudohypoaldosteronism patients with mutations in epithelial sodium channel (ENaC) subunit genes. *J. Steroid Biochem. Mol. Biol.* **2008**, *111*, 268–274. [[CrossRef](#)] [[PubMed](#)]
43. Edelheit, O.; Hanukoglu, I.; Shriki, Y.; Tfilin, M.; Dascal, N.; Gillis, D.; Hanukoglu, A. Truncated beta epithelial sodium channel (ENaC) subunits responsible for multi-system pseudohypoaldosteronism support partial activity of ENaC. *J. Steroid Biochem. Mol. Biol.* **2012**, *119*, 84–88. [[CrossRef](#)] [[PubMed](#)]
44. Drummond, H.A. ENaC proteins in vascular smooth muscle mechanotransduction. *Curr. Top. Membr.* **2007**, *59*, 127–153.
45. Drummond, H.A.  $\beta$ ENaC is a molecular component of a VSMC mechanotransducer that contributes to renal blood flow regulation, protection from renal injury, and hypertension. *Front. Physiol.* **2012**, *3*, 341. [[CrossRef](#)]
46. Chung, W.S.; Weissman, J.L.; Farley, J.; Drummond, H.A.  $\beta$ ENaC is required for whole cell mechanically gated currents in renal vascular smooth muscle cells. *Am. J. Physiol. Ren. Physiol.* **2013**, *304*, F1428–F1437. [[CrossRef](#)]
47. Baldin, J.P.; Barth, D.; Fronius, M. Epithelial Na<sup>+</sup> channel (ENaC) formed by one or two subunits forms functional channels that respond to shear force. *Front. Physiol.* **2020**, *11*, 141. [[CrossRef](#)]
48. Graudal, N.; Jürgens, G.; Baslund, B.; Alderman, M.H. Compared with usual sodium intake, low- and excessive-sodium diets are associated with increased mortality: A meta-analysis. *Am. J. Hypertens.* **2014**, *27*, 1129–1137. [[CrossRef](#)]
49. Mancia, G.; Oparil, S.; Whelton, P.K.; McKee, M.; Dominiczak, A.; Luft, F.C.; AlHabib, K.; Lanus, F.; Damasceno, A.; Prabhakaran, D.; et al. The technical report on sodium intake and cardiovascular disease in low- and middle-income countries by the joint working group of the World Heart Federation, the European Society of Hypertension and the European Public Health Association. *Eur. Heart J.* **2017**, *38*, 712–719. [[CrossRef](#)]
50. Lelli, D.; Antonelli-Incalzi, R.; Bandinelli, S.; Ferrucci, L.; Pedone, C. Association between Sodium Excretion and Cardiovascular Disease and Mortality in the Elderly: A Cohort Study. *J. Am. Med. Dir. Assoc.* **2018**, *19*, 229–234. [[CrossRef](#)]
51. Masilamani, S.; Wang, X.; Kim, G.H.; Brooks, H.; Nielsen, J.; Nielsen, S.; Nakamura, K.; Stokes, J.B.; Knepper, M.A. Time course of renal Na-K-ATPase, NHE3, NKCC2, NCC, and ENaC abundance changes with dietary NaCl restriction. *Am. J. Physiol. Ren. Physiol.* **2002**, *283*, F648–F657. [[CrossRef](#)] [[PubMed](#)]
52. Graudal, N.A.; Hubeck-Graudal, T.; Jurgens, G. Effects of low sodium diet versus high sodium diet on blood pressure, renin, aldosterone, catecholamines, cholesterol, and triglyceride. *Cochrane Database Syst. Rev.* **2011**, *9*, CD004022.
53. Soundararajan, R.; Pearce, D.; Ziera, T. The role of the ENaC-regulatory complex in aldosterone-mediated sodium transport. *Mol. Cell. Endocrinol.* **2012**, *350*, 242–247. [[CrossRef](#)] [[PubMed](#)]
54. Sutherland, G.R.; Bain, A.D. Culture of cells from the urine of newborn children. *Nature* **1972**, *239*, 231. [[CrossRef](#)] [[PubMed](#)]
55. Linder, D. Culture of cells from the urine and bladder washings of adults. *Somat. Cell Genet.* **1976**, *2*, 281–283. [[CrossRef](#)]
56. Felix, J.S.; Littlefield, J.W. Urinary tract epithelial cells cultured from human urine. *Int. Rev. Cytol. Suppl.* **1979**, *10*, 11–23.
57. Felix, J.S.; Littlefield, J.W. Human newborn urine as a source of epithelial cells. *Birth Defects Orig. Artic. Ser.* **1980**, *16*, 231–237.
58. Dörrenhaus, A.; Müller, J.I.F.; Golka, K.; Jedrusik, P.; Schulze, H.; Föllmann, W. Cultures of exfoliated epithelial cells from different locations of the human urinary tract and the renal tubular system. *Arch. Toxicol.* **2000**, *74*, 618–626. [[CrossRef](#)]
59. Rahmoune, H.; Thompson, P.W.; Ward, J.M.; Smith, C.D.; Hong, G.; Brown, J. Glucose transporters in human renal proximal tubular cells isolated from the urine of patients with non-insulin-dependent diabetes. *Diabetes* **2005**, *54*, 3427–3434. [[CrossRef](#)]
60. Abedini, A.; Zhu, Y.O.; Chatterjee, S.; Halasz, G.; Devalaraja-Narashimha, K.; Shrestha, R.; Balzer, M.S.; Park, J.; Zhou, T.; Ma, Z.; et al. Urinary Single-Cell Profiling Captures the Cellular Diversity of the Kidney. *J. Am. Soc. Nephrol.* **2021**, *32*, 614–627. [[CrossRef](#)]
61. Zhou, T.; Benda, C.; Dunzinger, S.; Huang, Y.; Ho, J.C.; Yang, J.; Wang, Y.; Zhang, Y.; Zhuang, Q.; Li, Y.; et al. Generation of human induced pluripotent stem cells from urine samples. *Nat. Protoc.* **2012**, *7*, 2080–2089. [[CrossRef](#)] [[PubMed](#)]
62. Zhang, D.; Wei, G.; Li, P.; Zhou, X.; Zhang, Y. Urine-derived stem cells: A novel and versatile progenitor source for cell-based therapy and regenerative medicine. *Genes Dis.* **2014**, *1*, 8–17. [[CrossRef](#)] [[PubMed](#)]
63. Manaph, N.P.; Al-Hawwas, M.; Bobrovskaya, L.; Coates, P.T.; Zhou, X.F. Urine-derived cells for human cell therapy. *Stem Cell Res.* **2018**, *9*, 189. [[CrossRef](#)] [[PubMed](#)]
64. Burdeyron, P.; Giraud, S.; Hauet, T.; Steichen, C. Urine-derived stem/progenitor cells: A focus on their characterization and potential. *World J. Stem Cell* **2020**, *12*, 1080–1096. [[CrossRef](#)]
65. Ben-David, U.; Siranosian, B.; Ha, G.; Tang, H.; Oren, Y.; Hinohara, K.; Strathdee, C.A.; Dempster, J.; Lyons, N.J.; Burns, R.; et al. Genetic and transcriptional evolution alters cancer cell line drug response. *Nature* **2018**, *560*, 325–330. [[CrossRef](#)]
66. Lu, T.J.; Kan, W.C.; Yang, S.S.; Jiang, S.T.; Wu, S.N.; Ling, P.; Bao, B.Y.; Lin, C.Y.; Yang, Z.Y.; Weng, Y.P.; et al. MST3 is involved in ENaC-mediated hypertension. *Am. J. Physiol. Renal. Physiol.* **2019**, *317*, F30–F42. [[CrossRef](#)]
67. Chan, C.H.; Wu, S.N.; Bao, B.Y.; Li, H.W.; Lu, T.L. MST3 Involvement in Na<sup>+</sup> and K<sup>+</sup> Homeostasis with Increasing Dietary Potassium Intake. *Int. J. Mol. Sci.* **2021**, *22*, 999. [[CrossRef](#)]